Challenges Associated with Adaptation to Future Urban Expansion

M. GEORGESCU

School of Geographical Sciences and Urban Planning, Arizona State University, Tempe, Arizona

(Manuscript received 22 April 2014, in final form 23 November 2014)

ABSTRACT

The most populated state in the United States, California, is projected to add millions of new inhabitants through the end of the current century, requiring considerable landscape conversion to the built environment. A suite of continuous multiyear, medium-range resolution (20-km grid spacing), ensemble-based simulations is examined to assess urban expansion climate effects on California in 2100, and potential strategies to alleviate them. Summertime [June–August (JJA)] warming due to urban expansion of 1°–2°C is greater relative to any other season, and is completely offset by a range of adaptation strategies: green roofs (highly transpiring), cool roofs (highly reflective), and hybrid roofs (with combined biophysical properties of green and cool roofs). After offsetting of urban-induced warming, cool and hybrid roofs lead to a further 1°–2°C reduction in JJA 2-m temperature, highlighting enhanced efficacy of these adaptation strategies. Guided by medium-range-resolution results, additional high-resolution (2-km grid spacing) experiments are conducted for a subset of the JJA periods conducted on a coarser scale. Urban-induced 1°–2°C warming (local maximum warming exceeds 4°C) is simulated, and is offset by cool and green roof deployment. In agreement with coarser-resolution results, maximum near-surface cooling is greater for cool roofs relative to green roofs. Reduced daytime warming associated with both cool and green roofs also modifies the convective mixed layer, reducing turbulent kinetic energy and planetary boundary layer height, although this impact is less for green roofs than for cool roofs. The results presented here demonstrate the importance of future urban expansion in California and illustrate climatic consequences with implications for regional air quality.

1. Introduction

Accommodating the needs of future U.S. inhabitants will necessitate substantial conversion of existing landforms to the built environment (e.g., residential dwellings, transportation network, and commercial infrastructure), prompting development of roughly 250 000 km^2 of new urban land use through 2100 (Bierwagen et al. 2010). A sizable fraction of projected urban growth is expected for the state of California—the most populated state in the United States—with a meaningful share of expansion located within its agriculturally productive central regions (Fig. 1). The state's Central Valley is of notable importance both locally (4 of the top 5 producing counties, in terms of agricultural cash receipts, are located within the Central Valley; USDA 2012) and domestically (California agriculture supplies over one-third of the country's vegetables and about two-thirds of the country's fruits and nuts; USDA 2012). Through 2060, the Central Valley population will account for nearly one-third of the 15 million additional state inhabitants (California Department of Finance 2013). Modification of large swaths of existing California landscapes to urban areas raises regional climate concerns for future residents.

Urban environments, perhaps the most evident expression of land-use and land-cover change, are recognized as major modifiers of local- to regional-scale climate (Mills 2007). While the urban heat island (UHI) is classically acknowledged as the most distinct indicator of the built environment's existence (Stewart and Oke 2012), examination of urban impacts must extend beyond near-surface temperature to include effects on hydroclimate, air quality and consequent dispersion of particulates, energy demand necessary for the maintenance of living comfort, and consequences for ecosystems and biodiversity (Shepherd 2005; Kaufmann et al. 2007; Hanna et al. 2006; Lawrence et al. 2007; Keirstead et al. 2012; Wu 2008; Salamanca et al. 2014). Potential impacts of greenhouse gas–induced climate change have

Denotes Open Access content.

Corresponding author address: Matei Georgescu, 975 S. Myrtle Ave., 5th floor, P.O. Box 875302, Tempe AZ 85287-5302.
E-mail: matei.georgescu@asu.edu

DOI: 10.1175/JCLI-D-14-00290.1

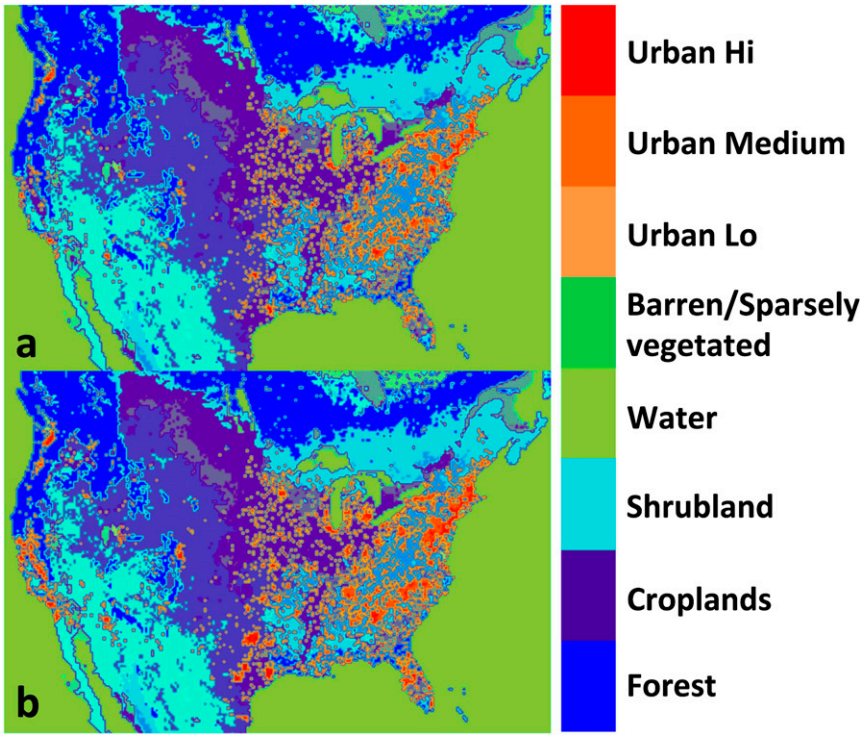

FIG. 1. Landscape representation for (a) Control (using ICLUS as 2000 urban representation) and (b) ICLUS_A2 denoting 2100 urban expansion.

received widespread research attention in California (e.g., Hayhoe et al. 2004; Cayan et al. 2008; Mahmud et al. 2008; Moser et al. 2009; Franco et al. 2011; Lobell and Field 2011; Zhao et al. 2011; Franklin et al. 2013; Pierce et al. 2013), while effects of urban areas as drivers of regional climate change have been less of a focus (LaDochy et al. 2007; Lebassi et al. 2009; Cordero et al. 2011). Because urban-induced climate change can be at least as important as greenhouse gas–induced climate change over regional scales (Adachi et al. 2012; Argüeso

TABLE 1. Description of medium-range-resolution simulations. Control: Control experiments, utilizing urban extent for year 2000. ICLUS_A2: Simulations utilizing projected ICLUS_A2 urban extent for year 2100. Cool roofs: As in ICLUS_A2 experiments, but with deployment of cool roofs for all urban areas. Green roofs: As in ICLUS_A2 experiments, but with deployment of green roofs for all urban areas. Hybrid roofs: As in ICLUS_A2 experiments, but with deployment of hybrid roofs for all urban areas. All simulations include three ensemble members, with variable spinup time. Analysis times (January 2001–December 2008) are identical.

Description of simulations	Spinup period	Analysis time
Control	January–December 2000	January 2001–December 2008
	July–December 2000	
	No spinup	
ICLUS_A2	January–December 2000	January 2001–December 2008
	July–December 2000	
	No spinup	
Cool roofs	January–December 2000	January 2001–December 2008
	July–December 2000	
	No spinup	
Green roofs	January–December 2000	January 2001–December 2008
	July–December 2000	
	No spinup	
Hybrid roofs	January–December 2000	January 2001–December 2008
	July–December 2000	
	No spinup	

TABLE 2. Description of high-resolution simulations. Control: Control experiments, utilizing urban extent for year 2000. ICLUS_A2: Simulations utilizing projected ICLUS_A2 urban extent for year 2100. Cool roofs: As in ICLUS_A2 experiments, but with deployment of cool roofs for all urban areas. Green roofs: As in ICLUS_A2 experiments, but with deployment of green roofs for all urban areas.

Description of simulations	Spinup period	Analysis time
Control	24–31 May 2001	1 Jun–31 Aug 2001
	24–31 May 2003	1 Jun–31 Aug 2003
	24–31 May 2005	1 Jun–31 Aug 2005
	24–31 May 2007	1 Jun–31 Aug 2007
ICLUS_A2	24–31 May 2001	1 Jun–31 Aug 2001
	24–31 May 2003	1 Jun–31 Aug 2003
	24–31 May 2005	1 Jun–31 Aug 2005
	24–31 May 2007	1 Jun–31 Aug 2007
Cool roofs	24–31 May 2001	1 Jun–31 Aug 2001
	24–31 May 2003	1 Jun–31 Aug 2003
	24–31 May 2005	1 Jun–31 Aug 2005
	24–31 May 2007	1 Jun–31 Aug 2007
Green roofs	24–31 May 2001	1 Jun–31 Aug 2001
	24–31 May 2003	1 Jun–31 Aug 2003
	24–31 May 2005	1 Jun–31 Aug 2005
	24–31 May 2007	1 Jun–31 Aug 2007

et al. 2014; Georgescu et al. 2013, 2014), effects resulting from the expanding urban environment, and strategies to alleviate them, require evaluation.

Hydroclimatic consequences of future U.S. megapolitan expansion have recently been examined and the efficacy of commonly proposed adaptation measures intended to diminish these impacts has been quantified (Georgescu et al. 2014). An extension of prior work, the focus here is on annually and spatially varying climate impacts resulting from projected end-of-century urbanization for California. Guided by previously conducted medium-range-resolution results, additional high-resolution experiments are performed to identify how simulated results depend on resolution, an essential determinant of modeling robustness. This is the first manuscript, to my knowledge, to quantify climate impacts for California due exclusively to anticipated urbanization.

The paper is organized as follows. Methods utilized are presented in section 2, including a description of medium- and high-resolution experiments, as well as observational data utilized for model evaluation. Section 3 presents the model evaluation for the high-resolution simulations. Urban expansion impacts, including modification of the diurnal cycle of near-surface temperature and modification of the daytime mixed and nighttime stable boundary layer, are also discussed in section 3. Results are summarized, conclusions are drawn, and guidance for future work is proposed in section 4.

2. Methods

a. Urban projections

Scenarios of urban expansion have been developed for the United States as part of the Environmental Protection Agency's (EPA's) Integrated Climate and

TABLE 3. Parameterizations and urban landscape categories used for high-resolution simulations.

WRF version	3.2.1
Horizontal (innermost) grid	ΔX and ΔY = 2 km
Number of grid points	201 (X direction), 257 (Y direction)
Vertical levels	30
Initialization time	0000 UTC 24 May (of respective year)
Terminal time	2100 UTC 31 August (of respective year)
Analysis time	0000 UTC 1 June–2100 UTC 31 August (of respective year)
Δt (innermost grid)	10 s
Radiation scheme	RRTM (longwave); RRTM for GCMs (RRTMG: shortwave)
Surface model	Noah
Cumulus scheme	Kain–Fritsch (turned on only for outer two grids)
Microphysics scheme	WSM3
PBL scheme	Mellor–Yamada–Janjic
Surface layer	Eta similarity
Urban representation	Three-category urban canopy model
	Urban low-intensity residential (0.70 urban; 0.30 vegetation)
	Urban high-intensity residential (0.85 urban; 0.15 vegetation)
	Urban commercial/industrial (0.95 urban; 0.05 vegetation)
	Canyon geometry
	Urban low-intensity residential: building height, 5 m; road width, 8.3 m; aspect ratio, 1.66
	Urban high-intensity residential: building height, 7.5 m; road width, 9.4 m; aspect ratio, 1.25
	Urban commercial/industrial: building height, 15 m; road width, 10.0 m; aspect ratio, 0.67
Initial and lateral boundary conditions	NCEP FNL

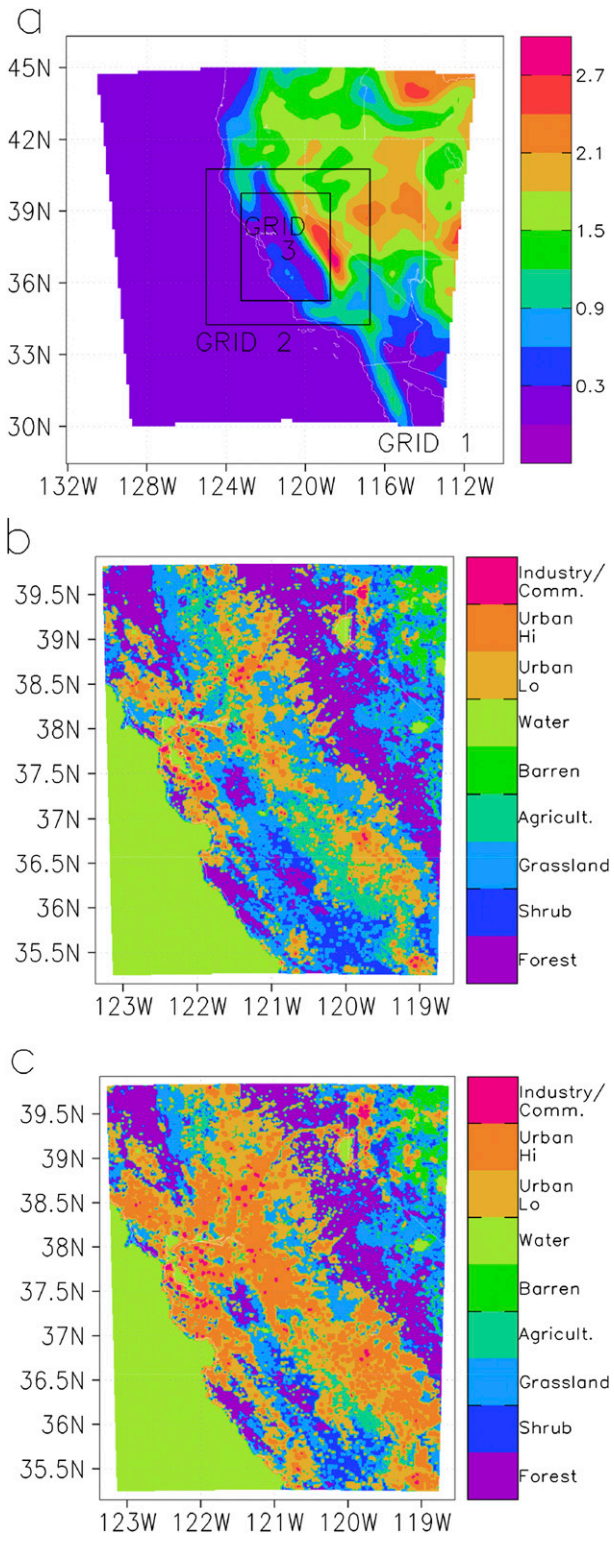

FIG. 2. (a) Geographical representation of the WRF nested grid configuration for high-resolution simulations, with topography overlaid (km). (b) Landscape representation for innermost domain (grid 3) utilizing 2000 urban representation. (c) As in (b), but utilizing projected ICLUS_A2 2100 urban representation.

Land Use Scenarios (ICLUS) project (Bierwagen et al. 2010). The ICLUS project accounts for domestic and international migrants for new county-based housing unit allocation at 1-ha resolution. Urban expansion projections are available at decadal frequency from 2000 through the end of the century for a low expansion scenario (whose population will likely be exceeded by the middle of the current century and will therefore not be discussed further) and a high expansion scenario (hereafter ICLUS_A2). The ICLUS urban extent for a 2000 baseline (hereafter Control) and ICLUS_A2 were mapped onto an existing urban classification for the regional climate model utilized in this work (Fig. 1, Table 1).

b. *Medium-resolution simulations: 20-km grid spacing*

Control and ICLUS_A2 urban categories were mapped onto the existing Noah land surface model classification scheme of the Advanced Research version of the Weather Research and Forecasting Model version 3.2.1 (WRF; Skamarock and Klemp 2008). A single-layer urban canopy model, accounting for urban geometry and associated radiation trapping, was used to simulate urban-related processes (e.g., modification to the surface energy balance) and feedbacks to the overlying atmosphere (Kusaka and Kimura 2004).

Continuous continental-scale simulations with 20-km grid spacing were conducted utilizing contemporary climate spanning 2001–08 with present (i.e., Control) and projected (i.e., ICLUS_A2) urban expansion. Each simulation was repeated an additional two times (i.e., 3 total members) through an altered initial start time, resulting in a different spinup time among the ensemble members. The 8-yr analysis time is identical for all experiments, enabling direct comparison. The National Centers for Environmental Prediction final analyses data (FNL) were used as initial and boundary conditions for all simulations. A full accounting of model options used and Control simulation performance has already been presented (Georgescu et al. 2014).

A trio of adaptation measures were undertaken to quantify the degree to which urban expansion impacts could be offset. First, ICLUS_A2 urban roofs were converted to "cool roofs": a commonly proposed UHI mitigation strategy whereby a greater fraction of incoming solar radiation is reflected to space (EPA 2008a), thereby lowering urban temperatures (e.g., Akbari and Matthews 2012; Synnefa and Santamouris 2012). Next, ICLUS_A2 urban roofs were converted to "green roofs": a UHI mitigation strategy that lowers urban canopy temperatures via enhanced evapotranspiration from vegetated rooftops (e.g., EPA 2008b; Sailor 2008; Yang

TABLE 4. Control simulation evaluation, temperatures presented for each of the four simulated summers (JJA). The following six stations were used: 1) Fresno Yosemite International Airport (36.78°N, 119.71°W), 2) Monterey Regional Airport NWS Forecast Office (36.5925°N, 121.8555°W), 3) Sacramento Executive Airport (38.56°N, 121.52°W), 4) San Francisco International Airport (37.66°N, 122.44°W), 5) San Jose International Airport (37.36°N, 121.92°W), and 6) Stockton Metropolitan Airport (37.89°N, 121.23°W). Model bias is in parentheses.

	Observations	WRF	Observations	WRF
	2001		2003	
Average (°C)	21.6	23.2 (+1.6)	22.2	24.0 (+1.8)
Maximum (°C)	28.6	28.9 (+0.3)	29.2	29.7 (+0.5)
Minimum (°C)	14.5	17.6 (+3.1)	15.3	18.4 (+3.1)
	2005		2007	
Average (°C)	21.8	23.5 (+1.7)	21.6	22.6 (+1.0)
Maximum (°C)	28.8	29.0 (+0.2)	28.5	28.1 (−0.4)
Minimum (°C)	14.9	18.0 (+3.1)	14.6	17.2 (+2.6)

and Wang 2014). Finally, a hypothetical strategy is proposed resulting from the biophysical combination of cool and green roofs (i.e., reflective vegetation; hereafter called hybrid roofs; Table 1).

c. *High-resolution simulations: 2-km grid spacing*

Guided by medium-range-resolution (20-km grid spacing) simulations (section 2b), additional 2-km grid spacing experiments were performed with the same version of WRF, for a subset of the 2001–08 period. Because medium-resolution-simulated impacts of urban expansion were largest during summer season (section 3b), the focus of all high-resolution simulations was chosen as June–August (JJA). Prior to execution of the high-resolution simulations four summers were selected, since computational limitations precluded the numerical integration of all eight summers at 2-km grid spacing. To account for the potential variability among different summers,

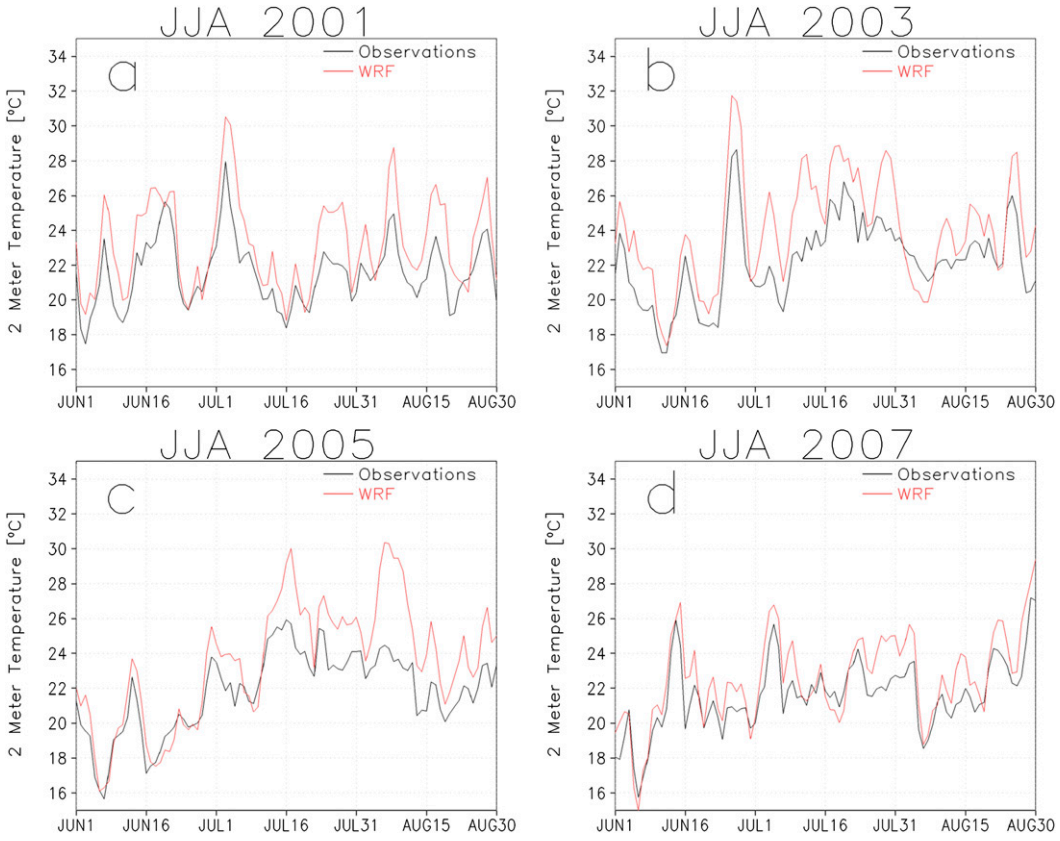

FIG. 3. Observed (black curve) and WRF-simulated (red curve) daily averaged time series of 2-m air temperature (°C) for (a) JJA 2001, (b) JJA 2003, (c) JJA 2005, and (d) JJA 2007.

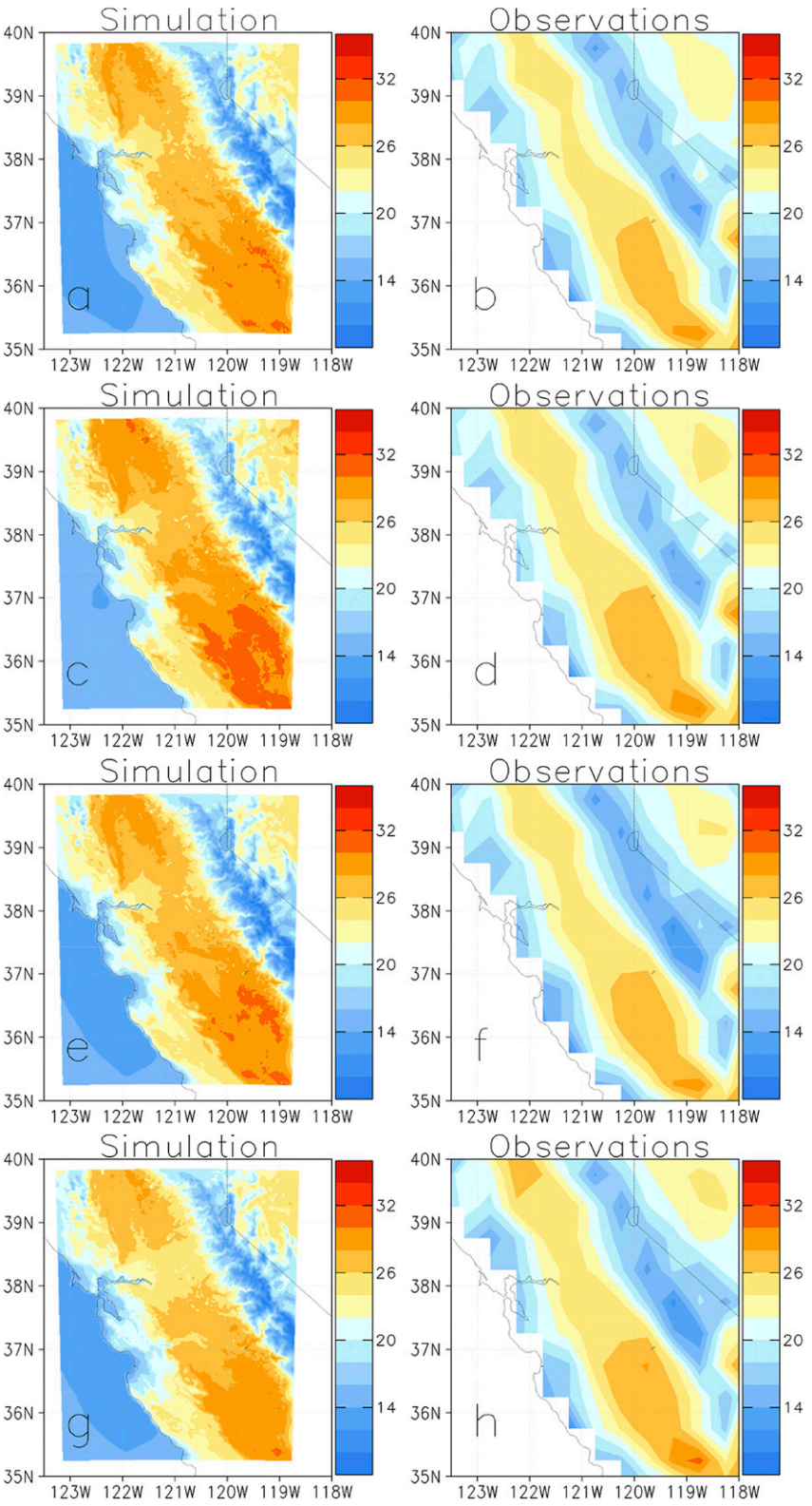

FIG. 4. WRF-simulated and observed JJA spatial mean of 2-m air temperature (°C) for (a),(b) 2001, (c),(d) 2003, (e),(f) 2005, and (g),(h) 2007. Observational dataset used is the University of Delaware global temperature dataset.

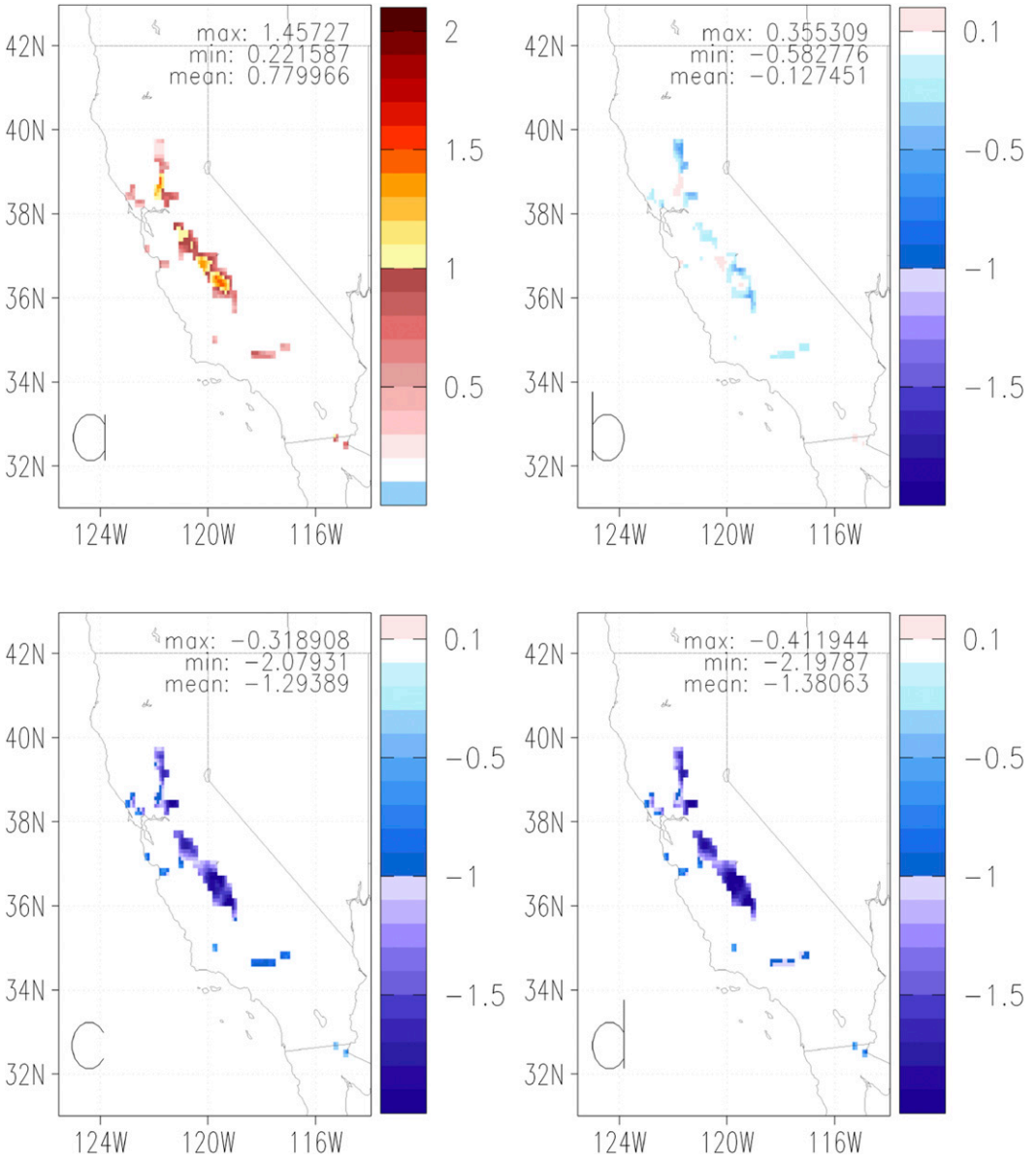

FIG. 5. Time-averaged (2001–08) simulated 2-m air temperature difference (°C) between (a) ICLUS_A2 and Control, (b) green roofs and Control, (c) cool roofs and Control, and (d) hybrid roofs and Control.

continuous JJA seasons (e.g., 2001–04) were not simulated. Instead, the methodological approach assumed the largest possible spread in simulated summer seasons and either the quartet, 2001, 2003, 2005, and 2007, or the quartet beginning in 2002 were deemed equally suitable. The initial quartet of JJA summers was selected (Table 2). All parameterizations and reanalysis data used for high-resolution simulations remained identical to the medium-resolution experiments (Table 3), and no model tuning of any kind was performed.

A triply nested grid configuration enabled dynamical downscaling from the synoptic flow field (grid 1: 32-km grid spacing) to the intermediate grid (grid 2: 8-km grid spacing) and further to the finest grid (grid 3: 2-km grid spacing). The center of all domains was positioned to coincide with the California area projected to undergo greatest expansion (i.e., the Central Valley region of the state; Fig. 2). All simulations were initialized on 24 May at 0000 UTC of the corresponding year and continued to 31 August at 2100 UTC of the equivalent year (Table 2). The initial week of all experiments was regarded as spinup and discarded. The analysis time, for all high-resolution experiments, was 1 June–31 August, for each of the four summers.

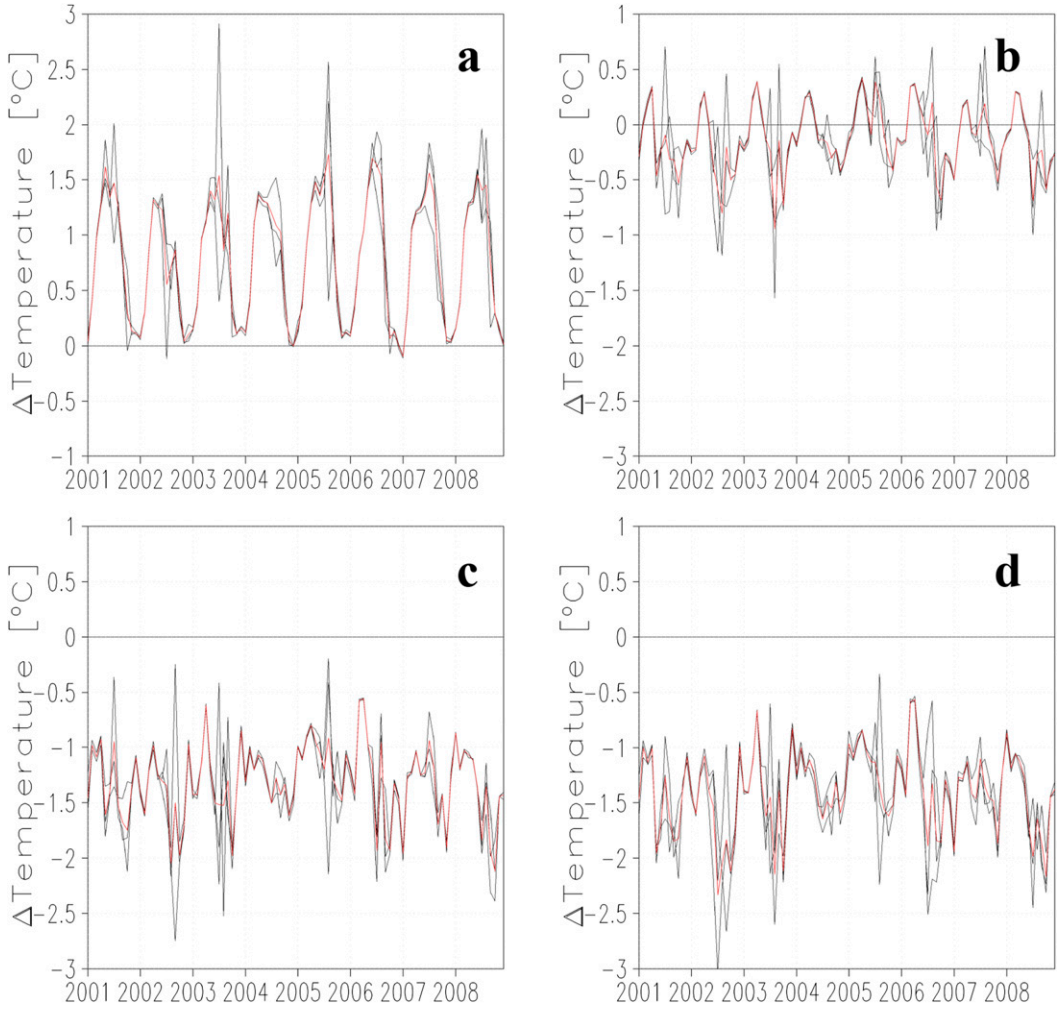

FIG. 6. Domain-averaged 2-m air temperature difference (°C; over pixels shown in Fig. 5) between (a) ICLUS_A2 and Control, (b) green roofs and Control, (c) cool roofs and Control, and (d) hybrid roofs and Control, for the extent of the simulation period (2001–08). Red curves for each panel depict ensemble mean difference and black curves show individual member differences. Note that the *y*-axis range is different for (a) relative to other panels.

The representation of current and future urban expanse, and adaptation strategies, in all high-resolution simulations was identical to those used for the 20-km grid spacing experiments. Control and ICLUS_A2 therefore represent contemporary and 2100 projected urban development. Likewise, cool roofs and green roofs were deployed over all ICLUS_A2 urban roofs. Because JJA climate impacts owing to the hybrid roofs technology did not indicate significantly different impacts compared to cool roofs (section 3b), this urban adaptation strategy was not further examined in the high-resolution experiments (Table 2).

d. Model evaluation data

The medium-resolution experiments revealed broad agreement with gridded observational data (Georgescu et al. 2014), but the additional high-resolution experiments require evaluation prior to sensitivity analysis. To accomplish this, both individual meteorological stations, as well as suitable gridded products, were utilized to assess time-varying and spatially explicit model performance.

Six meteorological stations from across the region were selected: Fresno, Monterey, Sacramento, San Francisco, San Jose, and Stockton, California (Table 4). Maximum and minimum daytime temperatures were retrieved for all stations for the 3-month (JJA) period of analysis for each of the four simulated summers. Station data were obtained from the National Climatic Data Center's Climate Data Online (http://www.ncdc.noaa.gov/cdo-web/search). Utility of meteorological stations enabled time-varying model performance. Although the high-resolution nature of the experiments (2 km on the

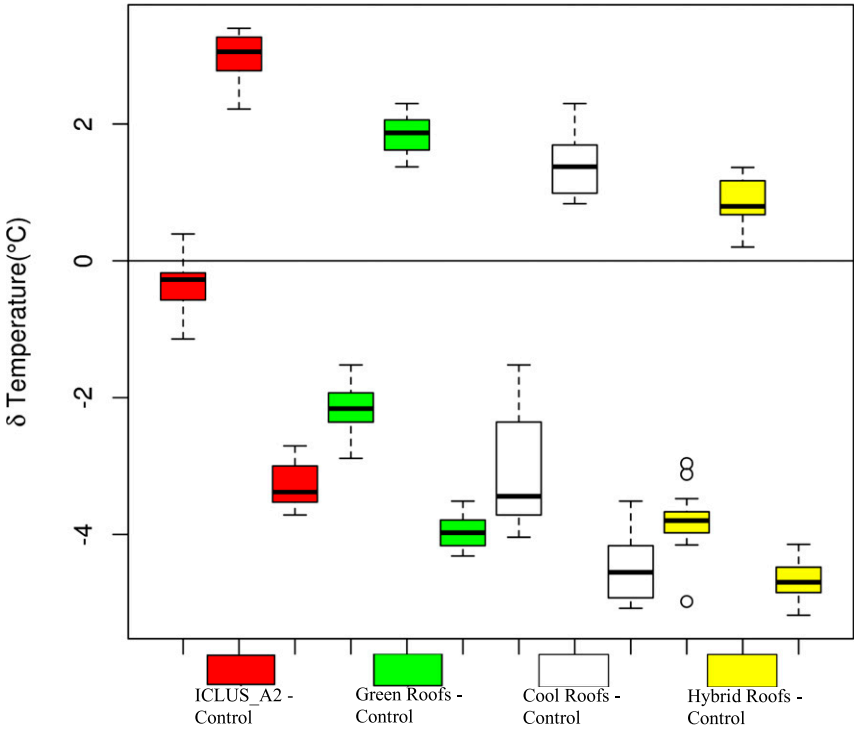

FIG. 7. Box-and-whisker plots of WRF-simulated impact on JJA 2 m daytime maximum (T_{max}; left of color trio), nighttime minimum (T_{min}; center of color trio), and diurnal temperature range ($T_{max} - T_{min}$; right of color trio) for ICLUS_A2 expansion (red), green roofs (green), cool roofs (white), and hybrid roofs (yellow), relative to Control.

innermost grid) is suitable for the current application, one cannot expect reasonable agreement between a model-resolved 4-km^2 grid cell and a station location covering an area of 1 m^2. For this reason, observations are averaged over all (six) stations and compared with the corresponding average of model-simulated, nearest grid point station locations.

To assess spatially explicit model performance the University of Delaware air temperature dataset, provided by the NOAA/OAR/ESRL Physical Sciences Division (PSD), Boulder, Colorado, from their website (http://www.esrl.noaa.gov/psd/data/gridded/data.UDel_AirT_Precip.html), was made. As with the meteorological stations, model performance was examined for each of the four simulated summers. Because precipitation is rarely observed during this time of year for this region, and the simulations correctly reproduced this feature (not shown), this variable was not considered further.

e. Statistical significance

The pairwise comparison test [PCT; von Storch and Zwiers 2002; see also the supplemental material of Georgescu et al. (2013)] was used to examine statistical significance of medium resolution results. According to the PCT, the probability that 19 or more of the 24-yr sample of experiments (or 24 seasons; 8 seasons multiplied by 3 ensemble members) will produce a trend of the same signal as the mean signal by chance is 0.3%. The criteria defined here is more stringent by additionally requiring warming exceeding 0.10°C relative to the mean signal. Statistical significance is calculated for annual differences and only those pixels where differences greater than 99% probability occur are used for subsequent analyses. Because of the limited sample size (four summers) the PCT was not used for the high-resolution simulations. Instead, the standard deviation of appropriate metrics is calculated to provide a quantitative sense of simulated variability.

3. Results

a. Model evaluation

The temporally varying WRF simulated daily averaged time series of near-surface temperature (2-m height above surface) shows good agreement compared to meteorological station observations (Fig. 3). Notably, the intrasummer tendency of near-surface temperature was well simulated for all four summers (i.e., when the observations indicated a sharp increase in temperature the

TABLE 5. Average summertime near-surface temperature (T), sensible heat flux (SH), ground heat flux (GRD), latent heat flux (LH), and PBL depth (PBL) for Control at 0000, 0600, 1200, and 1800 UTC (1700, 2300, 0500, and 1100 LST, respectively). Also shown are differences between each urban expansion/adaptation scenario less Control. All values correspond only to statistically significant urban grid cells illustrated in Fig. 5. Negative GRD absolute values indicate energy storage within urban areas.

	0000 UTC	0600 UTC	1200 UTC	1800 UTC
T (°C)				
Control	34	21	17	29
SH (W m^{-2})				
Control	239	−20	−14	370
GRD (W m^{-2})				
Control	−34	63	53	−101
LH (W m^{-2})				
Control	37	1	0	42
PBL (m)				
Control	1887	407	240	710
ΔT (°C)				
ICLUS_A2	−0.3	2.9	3.0	−0.2
Green roofs	−2.1	1.5	1.8	−1.7
Cool roofs	−3.7	0.6	1.1	−3.1
Hybrid roofs	−3.8	0.3	0.9	−3.3
ΔSH (W m^{-2})				
ICLUS_A2	3	26.4	18.4	−61.9
Green roofs	−58	14.8	13.3	−113
Cool roofs	−96	14.1	12.5	−155
Hybrid roofs	−96	11.4	11.0	−160
ΔGRD (W m^{-2})				
ICLUS_A2	−13	53	44	−93
Green roofs	−10	40	33	−69
Cool roofs	−9	24	25	−42
Hybrid roofs	−8	23	23	−40
ΔLH (W m^{-2})				
ICLUS_A2	−22	0	0	−25
Green roofs	71	14	7	72
Cool roofs	−17	0	0	−20
Hybrid roofs	−1	6	3	−13
ΔPBL (m)				
ICLUS_A2	−179.4	53.8	49.9	−43.3
Green roofs	−587.5	7.6	27.1	−140.8
Cool roofs	−921.3	−26.9	11.0	−249.1
Hybrid roofs	−947.7	−32.7	6.3	−258.1

model followed suit; conversely, when the observations indicated a sharp decrease in temperature, the model appropriately reproduced these changes). The model simulated deviation from averaged diurnal temperatures indicated an absolute temperature (warm) bias of 1°–2°C. The WRF simulated maximum temperature was in excellent agreement with observed maximum temperatures, with absolute error <1°C for all simulated summers (Table 4). However, simulated nighttime minimum temperatures revealed a positive bias, with nighttime minima generally 3°C warmer relative to observations. Potential reasons for general model disagreement compared to observations are likely related to the initial decision to not perform model tuning of any kind relative to the coarse-resolution experiments, therefore enabling a more direct identification of the degree of resolution independence. Indeed, had individual parameters been tuned to facilitate improved correspondence to observations, quantifying the degree of agreement between coarser- and higher-resolution adaptation simulations would have been less feasible. Further, and relevant to the primary motivation of this work, the apparent bias present in the Control simulations is likely to persist for the urban expansion and adaptation experiments, and differences between them will result in their cancelation. Nonetheless, the level of agreement for the simulated summers is deemed satisfactory to move forward with simulated examination of the model's spatial performance.

Figure 4 presents the JJA time-averaged mean of near-surface temperature for the WRF simulations alongside gridded observations available from the University of Delaware global temperature dataset for all four simulated summers. The spatial variability of simulated temperatures is well reproduced, with highest values along the extent of the Central Valley and lowest values along the higher terrain of the Sierra Nevada. In addition, the lower temperatures along the coastal California regions, including the San Francisco and Monterey Bay regions, are reasonably simulated.

Overall, the WRF simulated spatially and temporally averaged representation of thermal characteristics, for a suite of summer seasons, compares favorably with station and gridded product data, and provides confidence in the model's ability to suitably represent near-surface thermal patterns for this region.

b. *Climate impacts: 20-km grid spacing simulations*

Annually averaged near-surface temperature changes owing to projected urban expansion in excess of 1°C are widespread over the Sacramento and San Joaquin River valleys (Fig. 5a). Mean warming resulting from urban expansion is nearly 0.8°C, although spatial variability highlights the spectrum of simulated impacts ranging between 0.25° and 1.5°C. The potential to reduce urban environment–induced warming varies by adaptation technology (Figs. 5b–d). Widespread adoption of green roofs, on average, offsets urban-induced warming, although spatial heterogeneity is evident as some warming due to urban expansion lingers. Deployment of cool roofs eliminates urban-induced warming everywhere, leading to further annually averaged cooling of 1°–2°C. The performance of cool and hybrid roofs is spatially and quantitatively similar and only slight additional cooling (relative to cool roofs) is simulated when the biophysical characteristics of cool and green roofs are combined into the hybrid roof technology.

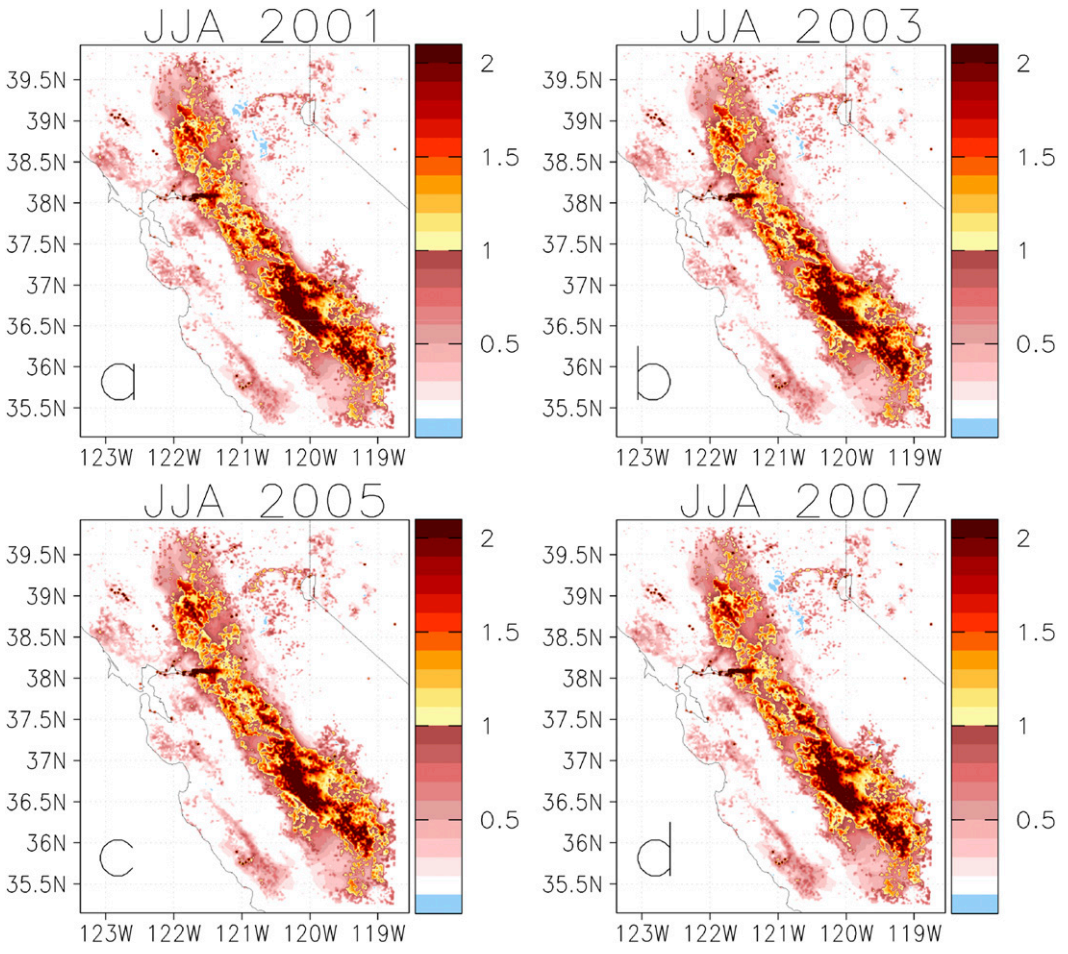

FIG. 8. Time-averaged simulated 2-m air temperature difference (°C) between ICLUS_A2 and Control for (a) JJA 2001, (b) JJA 2003, (c) JJA 2005, and (d) JJA 2007.

In addition to spatially averaged differences, it is necessary to characterize the time-varying evolution of near-surface temperature impacts. Figure 6 shows spatially averaged (over the statistically significant grid cells presented in Fig. 5) temperature differences between the urban expansion/adaptation experiments and Control. Simulated temperature differences owing to urban expansion illustrate seasonal fluctuation with maximum ensemble-averaged warming of approximately 1.5°C (red contour) peaking during the summer season. Urban-induced warming during spring and fall is reduced (generally less than 1°C). Winter season changes are minimal because of the dominant large-scale synoptic flow pattern. While variability is evident among individual ensemble members (black contours), therefore highlighting the degree of simulated uncertainty, the oscillatory nature of megapolitan-induced warming consistently occurs for the extent of the nearly decade-long period. The capacity to reduce urban-induced warming via green roofs also displays seasonal dependency as maximum cooling (~ -0.5°C) is simulated during the summer season, coinciding with the period of greatest urban-induced warming (i.e., maximum alleviation of urban-induced warming occurs during the season when it is required most). The summertime temperature decrease of approximately 0.5°C is a generally consistent feature, although year-to-year and intraensemble variability is evident. Finally, cool and hybrid roofs reduce near-surface temperatures throughout the year, with maximum efficiency during summer, resulting in an offset of urban-induced warming and ensuing cooling ranging between 1° and 2°C.

Given the significant mean summertime impacts identified, it is valuable to also assess the diurnal cycle of near-surface temperature changes. Figure 7 presents the simulated impact on JJA daytime maximum (T_{max}), nighttime minimum (T_{min}), and diurnal 2-m temperature range (DTR; $T_{max} - T_{min}$) for ICLUS_A2 and associated adaptation approaches. Consistent with prior work focusing on urbanization over semiarid regions (Georgescu et al. 2011), urban environment–induced

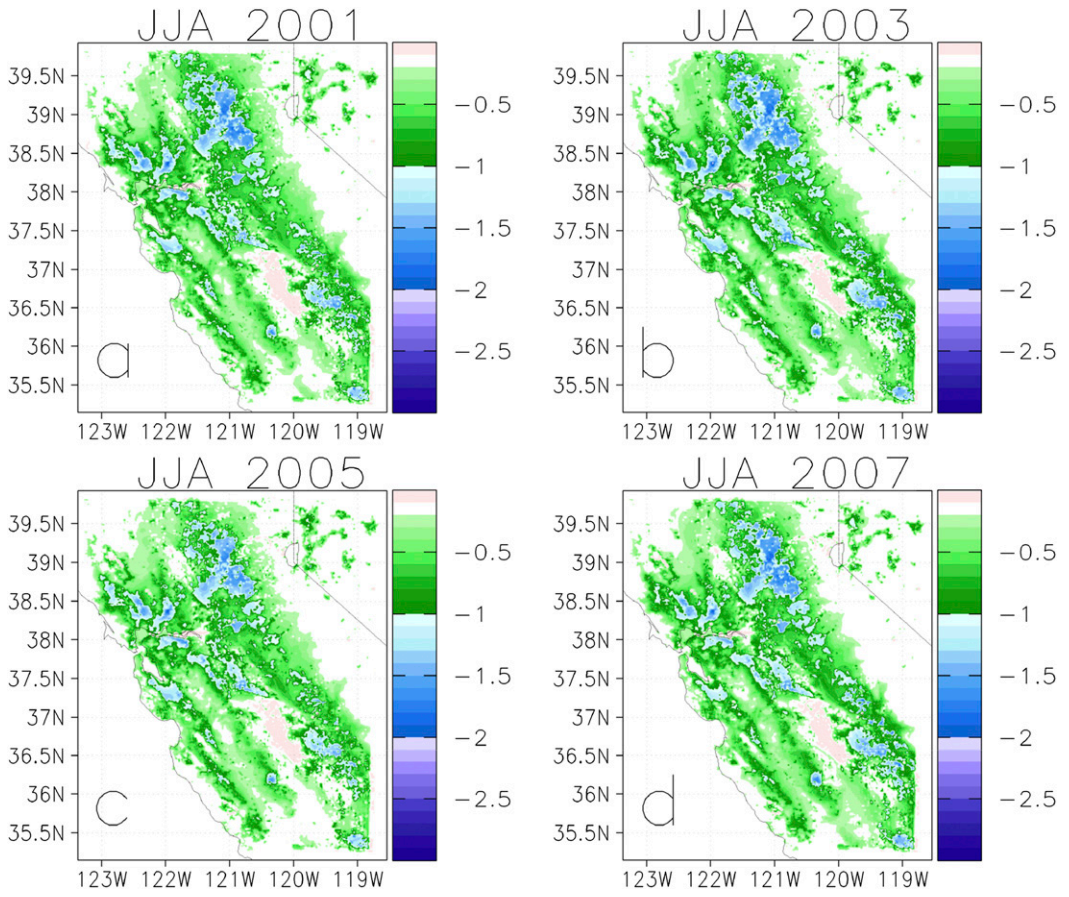

FIG. 9. Time-averaged simulated 2-m air temperature difference (°C) between green roofs and Control for (a) JJA 2001, (b) JJA 2003, (c) JJA 2005, and (d) JJA 2007.

climate change (i.e., the impact of the physically expanding urban infrastructure) can reduce daytime maximum temperatures (uncertainty among the 24 simulated summers envelops $\Delta T_{max} = 0°C$) because of increased urban environment energy storage by urban structures (Grimmond and Oke 1999; Table 5). The full range of simulated variability of urban expansion on T_{min} ranges between 2° and 3°C, illustrative of the predominantly nighttime warming influence associated with UHIs (Karl et al. 1988). The net effect of changes in T_{min} and T_{max} reduces the DTR by more than 3°C, a result that is amplified for all adaptation strategies.

It is important to examine historically observed DTR changes for California to provide context for our forward-looking analysis. Observed T_{min} and T_{max} changes demonstrate enhanced T_{min} relative to T_{max} warming trends for the San Joaquin and Sacramento River valley regions (Cordero et al. 2011). The authors highlight varying observed T_{max} trends (based on 1970–2006 data) obtained from the U.S. Historical Climate Network relative to the National Weather Service Cooperative Network (COOP), whereby a greater relative percentage of COOP stations exhibit summertime T_{max} cooling trends. Although a large fraction of these stations are located along the coast (e.g., Lebassi et al. 2009), several are situated within central California (LaDochy et al. 2007). LaDochy et al. (2007) show both observed positive and negative T_{max} urban trends, in contrast to the spatial and quantitative consistency identified for increasing T_{min} trends. The results presented here are therefore consistent with historically observed changes in T_{min} and T_{max} for urban areas within California, suggesting considerably greater impacts on minimum relative to maximum temperatures. To my knowledge regional modeling or remote sensing attribution studies examining the effect of historical, distinct land use conversion themes (e.g., Georgescu et al. 2009; Myint et al. 2013) have not been performed for California, but could provide insight into the roles of a range of forcings (e.g., the conversion of agricultural to urban landscapes) responsible for past temperature changes.

Finally, planetary boundary layer (PBL) changes indicate greater daytime relative to nighttime changes for the adaptation scenarios considered (Table 5). The

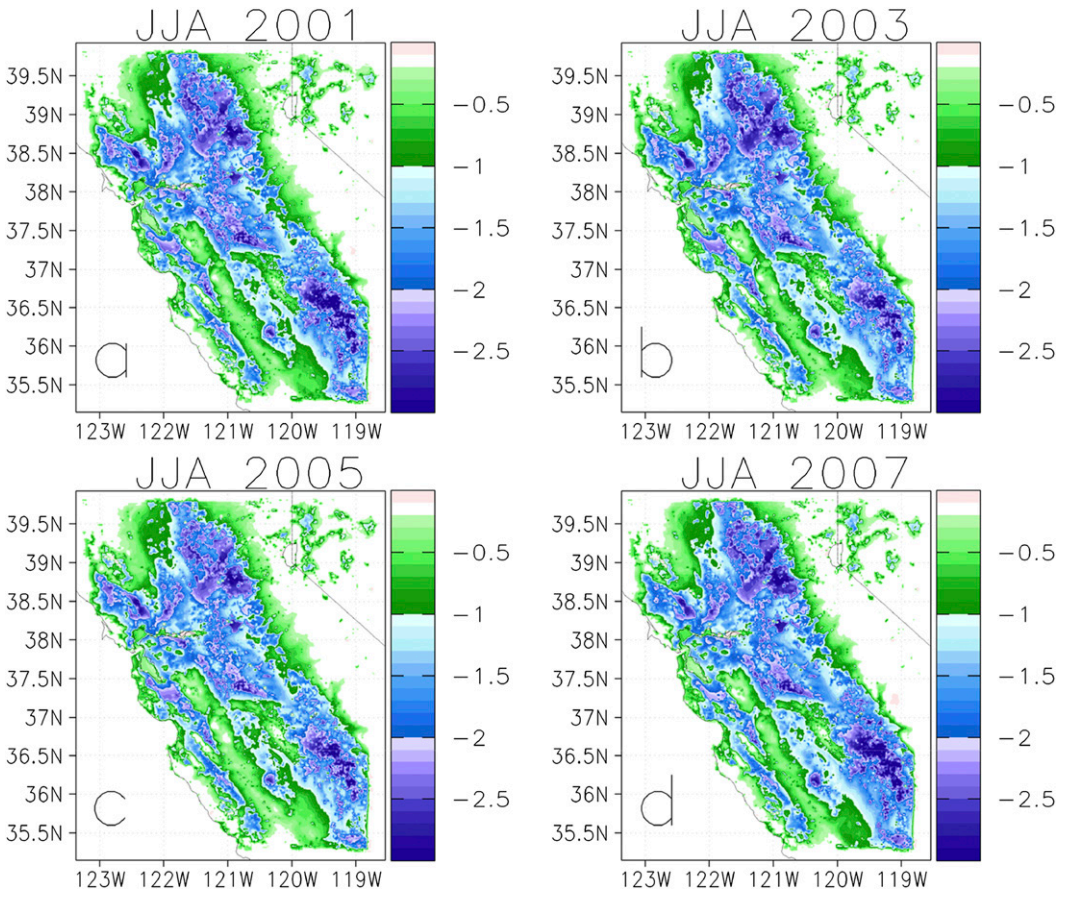

FIG. 10. Time-averaged simulated 2-m air temperature difference (°C) between cool roofs and Control for (a) JJA 2001, (b) JJA 2003, (c) JJA 2005, and (d) JJA 2007.

simulated Control magnitude of late afternoon PBL height for the Central Valley of California of 1887 m (Table 5) agrees with previous results ranging from 1750 m (observations; Zhao et al. 2009) to 2 km (simulations; Kueppers and Snyder 2012). The small reduction in daytime PBL depth is generally consistent with relatively minor impacts on T_{max} for ICLUS_A2 (mean reduction of 0.3°C for urban areas). Deployment of green, cool, and hybrid roofs, however, highlights the increased magnitude of PBL depth reduction of more than 500 m, with cool roofs displaying a pronounced depth decrease approaching 1 km. These results are in agreement with assessments focused on current urban extent showing reduced mixing height from increased built environment reflectivity (Taha 2008a,b). The magnitude of the adaptation impacts on PBL depth presented here is quantitatively similar to that of effects owing to present-day Central Valley irrigation (Kueppers and Snyder 2012).

c. *Climate impacts: 2-km grid spacing simulations*

Guided by results presented in the preceding section, the focus of the high-resolution simulations is restricted to the summer season. Figure 8 shows JJA-averaged near-surface temperature differences between ICLUS_A2 and Control simulations for each of the four simulated summers. Consistent with coarser-resolution results, urban-induced warming of 1°–2°C is simulated for the majority of locales undergoing urban development (cf. Figs. 2b and 2c, which illustrate the regions undergoing landscape conversion to the built environment). Notable exceptions are coastal locations, where warming is generally restricted to less than 1°C. Locally, maximum warming is simulated within the San Joaquin River valley, with peak warming exceeding 4°C for some locales. The overall impact of this urban expansion scenario is remarkably consistent among the four simulated summers.

Widespread adoption of green (Fig. 9) and cool (Fig. 10) roofs demonstrates the capability of these urban adaptation strategies to offset warming owing to expansion. For both strategies, cooling effects are not restricted to locales where the adaptation technology is deployed, instead indicating widespread cooling over large portions of the simulated domain. Spatial heterogeneity is evident for both strategies as maximum cooling is primarily limited to

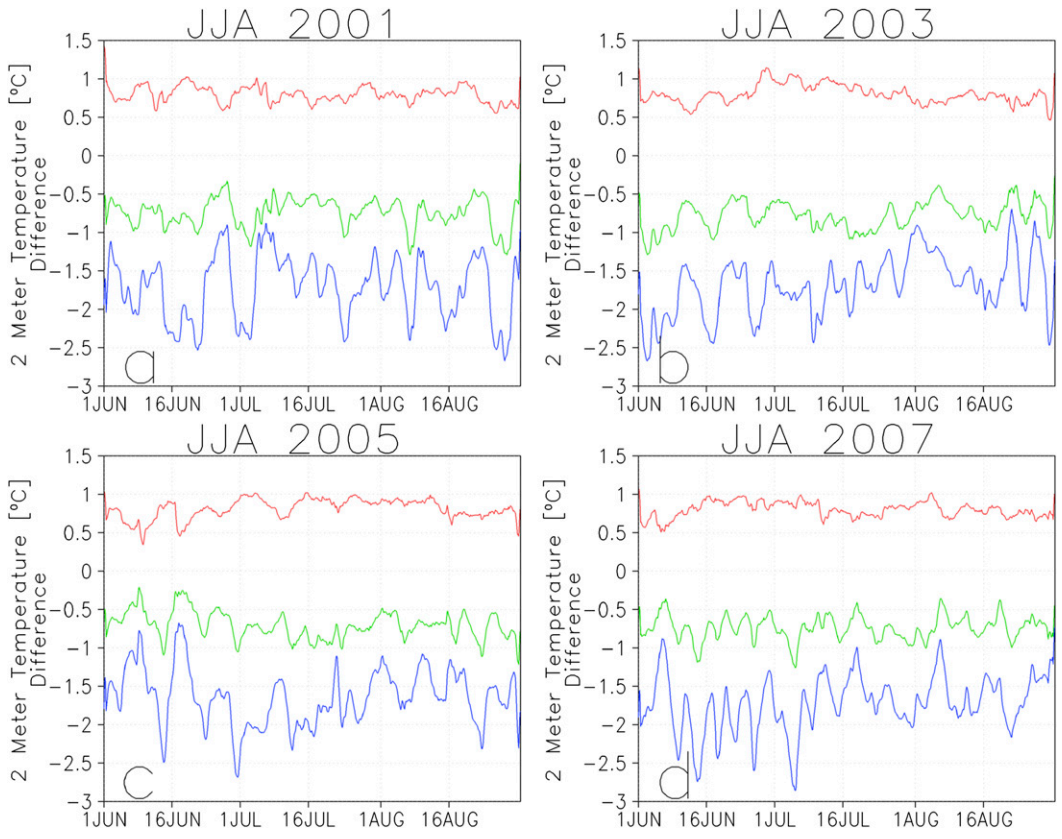

FIG. 11. WRF-simulated time series of domain-averaged 2-m daily air temperature difference (°C) between ICLUS_A2 and Control (red curve), green roofs and Control (green curve), and cool roofs and Control (blue curve) for (a) JJA 2001, (b) JJA 2003, (c) JJA 2005, and (d) JJA 2007. Calculations are performed only for urban grid cells.

urban areas. Deployment of green roofs leads to widespread cooling of urban regions although, consistent with the coarser-resolution simulations, some warming due to urban expansion lingers (Fig. 9). For all simulated summers, averaged cooling for urban grid cells resulting from green roof deployment leads to a further reduction of near-surface temperature of −0.74° (JJA 2001), −0.78° (JJA 2003), −0.71° (JJA 2005), and −0.74°C (JJA 2007), indicating somewhat greater cooling efficiency of green roofs relative to calculations made at the coarser resolution (see Fig. 5b). Deployment of cool roofs leads to similar widespread cooling over most of the land-based simulated domain (except for the higher terrain of the Sierra Nevada; Fig. 10). Spatial heterogeneity is apparent with decreased cooling (generally less than 1°C) over regions that did not undergo urbanization compared to further simulated cooling for urban grid cells (after offsetting of urban-induced warming) of 1°–3°C. For all simulated summers, averaged cooling for urban grid cells resulting from cool roof deployment leads to reduction of near-surface temperature of −1.72° (JJA 2001), −1.7° (JJA 2003), −1.64° (JJA 2005), and −1.72°C (JJA 2007), once again indicating greater cooling efficiency relative to calculations made at the coarser resolution (see Fig. 5c), and enhanced cooling efficiency compared to green roofs.

The JJA time series of diurnally averaged near-surface temperature differences, averaged only for urban grid cells, between the urban expansion (or adaptation scenarios) and the Control experiment further demonstrate variations in cooling potentials of green and cool roofs (Fig. 11). Such differences—generally about 1°C greater cooling for cool roofs relative to green roofs, but in both cases considerably offset urban-induced warming—could translate to substantial economic energy savings (e.g., Akbari et al. 2009; Oleson et al. 2010; Santamouris et al. 2011; Georgescu et al. 2014). These differences, largely consistent across the different JJA periods, persist for the duration of the summer. An important question that requires examination is how, and to what extent, these adaptation strategies impact the diurnal cycle of near-surface temperature. Impacts of urbanization, consistent with coarser-resolution results, indicate greater nighttime than daytime effects on near-surface temperature (Fig. 12a). The high-resolution simulations also show the expanding urban environment can reduce daytime maximum temperatures—although the magnitude is

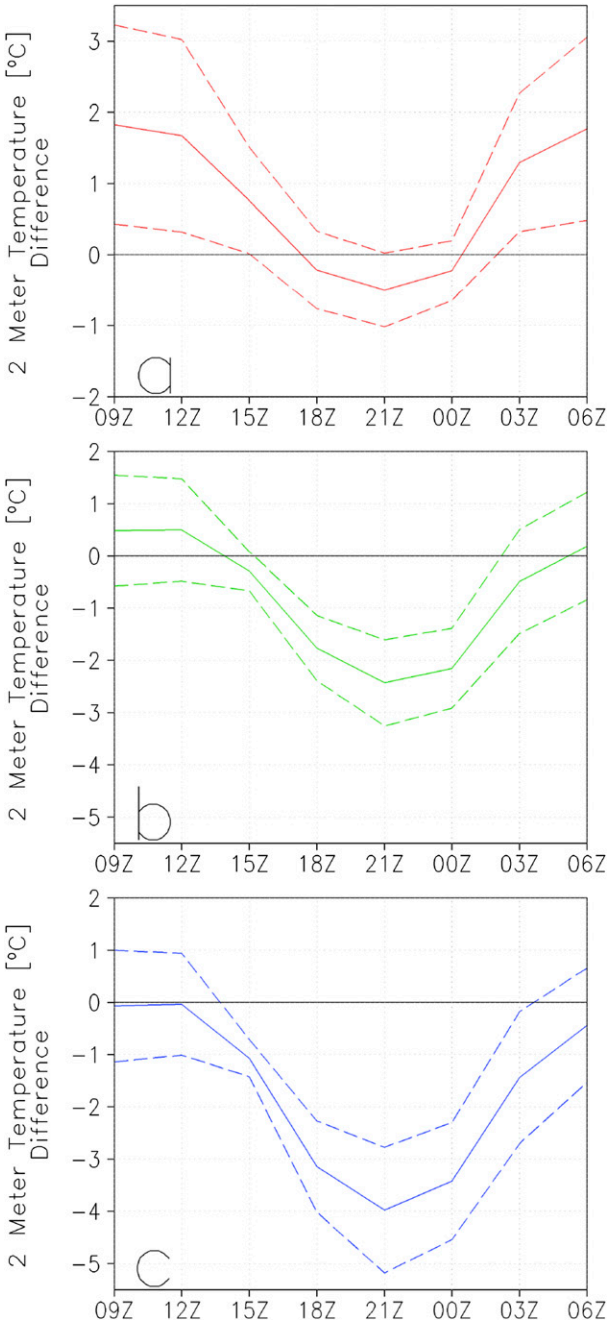

FIG. 12. WRF-simulated time series of diurnally averaged 2-m air temperature difference (°C), averaged across all four simulated summers (2001, 2003, 2005, and 2007), between (a) ICLUS_A2 and Control (red solid curve), (b) green roofs and Control (green solid curve), and (c) cool roofs and Control (blue solid curve). Dashed lines represent the corresponding ±1 standard deviation relative to mean difference displayed by the solid curves. Calculations are performed only for urban grid cells.

small compared to nighttime warming (Table 6)—with urban infrastructure energy storage once again assuming an important role (Table 6). Although the impact of urban development is greatest during evening and nighttime hours, effects of both adaptation strategies are greatest during daytime hours, when the warming influence of urban expansion is least (Fig. 12). Because of reduced impacts during nighttime hours (although, the deployment of green roofs does indicate mean nighttime warming peaking at 0.5°C; see Fig. 12b and Table 6), both adaptation strategies, via their considerable reduction of daytime maximum temperature, further reduce the DTR. The decrease in DTR associated with cool roofs has also been identified for urbanizing regions within the semiarid Sonoran Desert (Georgescu et al. 2013). The decrease in DTR associated with urban development, and further amplified by green and cool roofs, could have important implications for plant and animal communities and for power generation, as the timing (rather than just the diurnal-averaged magnitude) of energy demand reduction is essential.

Finally, although the emphasis until now has been on near-surface impacts, it is important to examine effects within the lower portions of the atmosphere. Figure 13 shows an altitude–longitude cross section of averaged turbulent kinetic energy (TKE) difference, at 36.75°N, between the urban expansion (or adaptation scenarios) and the Control experiment, from the first model layer extending to the free atmosphere. This transect coincides with a region of substantial projected urban expansion over the San Joaquin River valley (see Figs. 2b,c). The small decrease in TKE associated with urban expansion is consistent with slightly lower daytime near-surface temperatures, and therefore reduced buoyancy and a shallower PBL depth (Table 6). These impacts are of similar order of magnitude as simulated effects during evening hours, by which time the UHI is in full effect. By 0300 UTC, the warming impact resulting from urban expansion has surpassed 1°C, and maximum TKE differences (between ICLUS_A2 and Control experiments) are in excess of $0.5\,m^2\,s^{-2}$, effectively slowing the normal transition to a stable nighttime boundary layer. These results are in agreement with recent numerical experiments demonstrating reduced evening and nighttime vertical stability owing to warming associated with air conditioning usage (Salamanca et al. 2014).

Adaptation to urban expansion results in quantitatively larger daytime reduction in TKE, with peak reduction of -1.11 and $-1.41\,m^2\,s^{-2}$ for green (Fig. 13c) and cool (Fig. 13e) roofs, respectively. Although averaged and peak reduction is enhanced for cool relative to green roofs, both adaptation approaches increase the daytime stability of the lower atmosphere, leading to considerable PBL depth decrease (Table 6).

TABLE 6. As in Table 5, but for Control experiment across diurnal cycle: 0000, 0300, 0600, 0900, 1200, 1500, 1800, and 2100 UTC (1700, 2000, 2300, 0200, 0500, 0800, 1100, and 1400 LST, respectively). All calculations correspond to grid cells undergoing urbanization (see Fig. 2).

	0000 UTC	0300 UTC	0600 UTC	0900 UTC	1200 UTC	1500 UTC	1800 UTC	2100 UTC
T (°C)								
Control	32.7	27.5	23.1	21.0	19.2	22.3	28.4	32.4
SH (W m^{-2})								
Control	232	6	−1	0	−2	102	328	395
GRD (W m^{-2})								
Control	−29	109	98	87	78	−48	−169	−151
LH (W m^{-2})								
Control	41	4	1	0	0	22	52	59
PBL (m)								
Control	1431	477	335	237	182	357	773	1256
ΔT (°C)								
ICLUS_A2	−0.2	1.3	1.8	1.8	1.7	0.8	−0.2	−0.5
Green roofs	−2.2	−0.5	0.2	0.5	0.5	−0.3	−1.8	−2.4
Cool roofs	−3.4	−1.4	−0.4	−0.1	0	−1.1	−3.1	−4.0
ΔSH (W m^{-2})								
ICLUS_A2	8	32	19	15	12	−5	−48	−40
Green roofs	−87	3	5	7	6	−28	−125	−158
Cool roofs	−130	1	5	7	7	−52	−194	−232
ΔGRD (W m^{-2})								
ICLUS_A2	0	54	40	34	31	−18	−74	−63
Green roofs	−1	33	22	19	18	−22	−38	−29
Cool roofs	−11	3	5	8	11	15	−6	−20
ΔLH (W m^{-2})								
ICLUS_A2	−25	−2	−1	0	0	−13	−31	−36
Green roofs	106	31	16	10	7	18	113	158
Cool roofs	−22	−2	−1	0	0	−12	−29	−32
ΔPBL (m)								
ICLUS_A2	−41	187	59	59	43	34	−8	−63
Green roofs	−347	−16	−11	10	11	−21	−132	−315
Cool roofs	−618	−91	−44	−12	−5	−95	−264	−552

To test against the possibility that the selected transect was an outlier, we have examined additional cross sections to ensure these effects are not location specific. Figure 14 presents a similar altitude–longitude cross section of averaged TKE difference, but this time at 38.5°N. This transect coincides with extensive conversion to urban land cover over the Sacramento River valley (see Figs. 2b,c). Consistent with simulated impacts over the southern portion of the domain, conversion to urban land use results in a modest TKE decrease during the daytime. The effect of the urban adaptation strategies investigated here illustrates significant daytime mixing reduction within the PBL. Green roofs deployment reduces PBL depth by roughly 300 m during late afternoon hours, whereas the deployment of cool roofs essentially doubles PBL depth reduction (Table 6).

4. Discussion and conclusions

Impacts on climate for end-of-century urban expansion and adaptation have been examined for California through assessment of annual, seasonal, and summertime diurnal variability of appropriate climate metrics (e.g., PBL depth and DTR changes) for a suite of medium-range-resolution (20 km) and high-resolution (2 km) simulations. Results demonstrate near-surface temperature benefits resulting from cool, green, and hybrid roof deployment. Changes in simulated convective mixed layer characteristics, and consequently, a much shallower PBL depth, illustrate a key concern associated with diminished daytime turbulence: identical emissions of pollutants [e.g., particulate matter (PM)] will be confined to a smaller volume, thereby decreasing perceivable air quality. A shallower PBL can influence air quality (e.g., ozone and PM) positively or negatively depending on a host of other conditions. For example, additional modifications (e.g., to solar radiation, relative humidity/water vapor, ratios of volatile organic compounds to nitrous oxides, or wind speed and circulation) are likely to play further roles that could compensate for the decrease in PBL depth. If less solar radiation is absorbed because of cool roof deployment, reduced ozone production may be expected. Therefore, reliable air quality assessment of projected

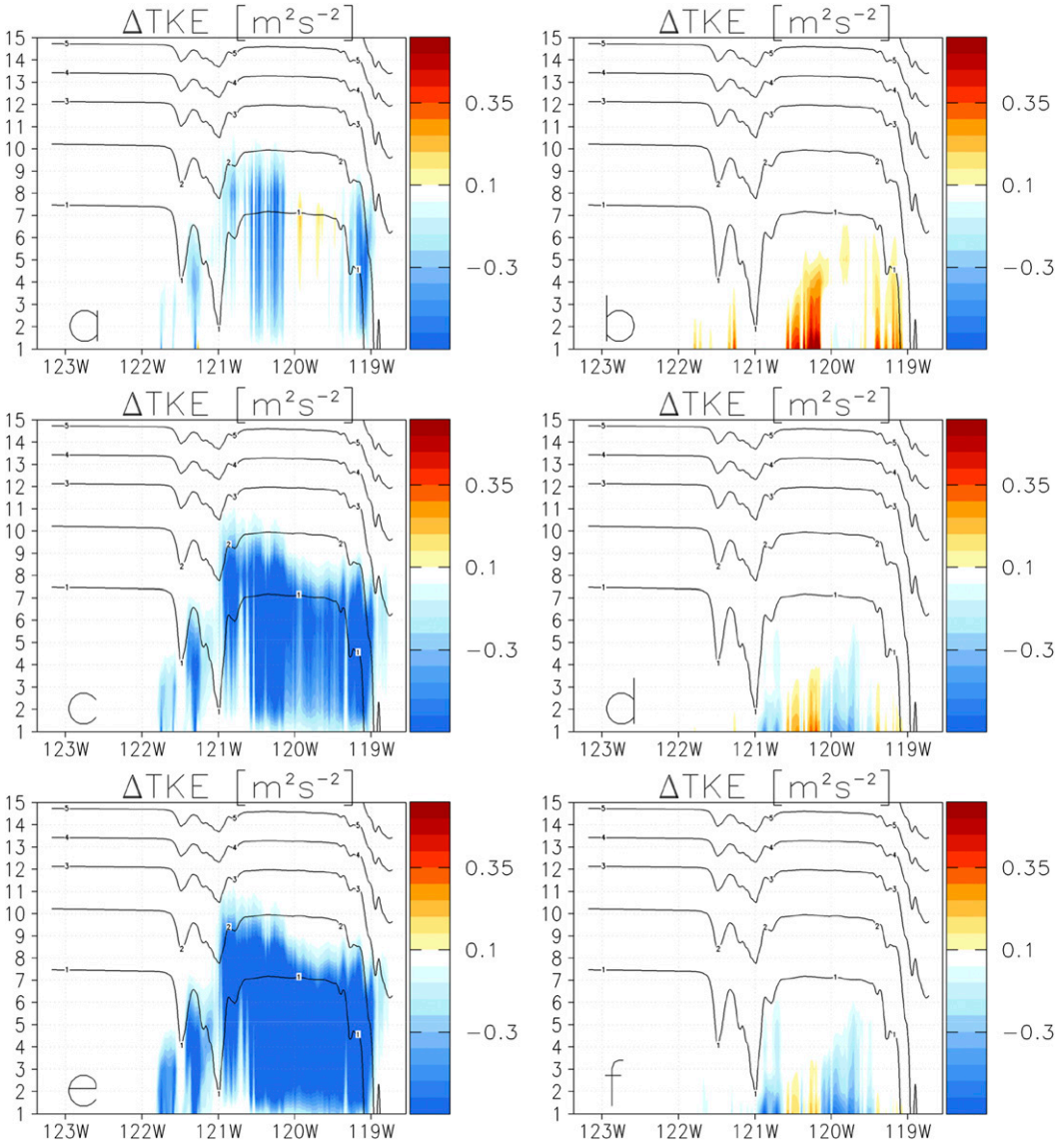

FIG. 13. WRF-simulated altitude–longitude cross section of averaged (across all simulated summers) turbulent kinetic energy (TKE) difference ($m^2 s^{-2}$) between ICLUS_A2 and Control at (a) 2100 and (b) 0300 UTC (1400 and 2000 LT, respectively). (c),(d) As in (a),(b), but for difference between green roofs and Control. (e),(f) As in (a),(b), but for difference between cool roofs and Control. Cross section is calculated at 36.75°N. The black contours in each panel indicate model height above sea level (km). The ordinate for each panel indicates the model level.

widespread conversion to the built environment will require the use of interactively coupled atmosphere–chemistry modeling tools (Jacobson 2001; Li et al. 2014) that also account for projected increases in emissions and future caps and energy control measures.

This work establishes the importance of future urban expansion and adaptation for California climate. However, it does not explicitly consider radiative effects associated with building precursor emissions (e.g., Gurney et al. 2012) or heating effects due to a variety of transit/transportation systems (e.g., Chester et al. 2013), which are likely to modify conditions beyond those presented here. For example, while a diurnal anthropogenic heating profile has been incorporated into the urban canopy scheme (Georgescu et al. 2014), potential changes in energy and fuel efficiency are likely to adjust this profile, and could aggravate or improve conditions. Establishing optimal reflectivities without generating unintended consequences (e.g., Georgescu et al. 2012, 2014), coupled with high emissivity materials (e.g., Santamouris et al. 2011) and a preferred landscape configuration (Connors et al. 2013) that permits longwave radiation loss during

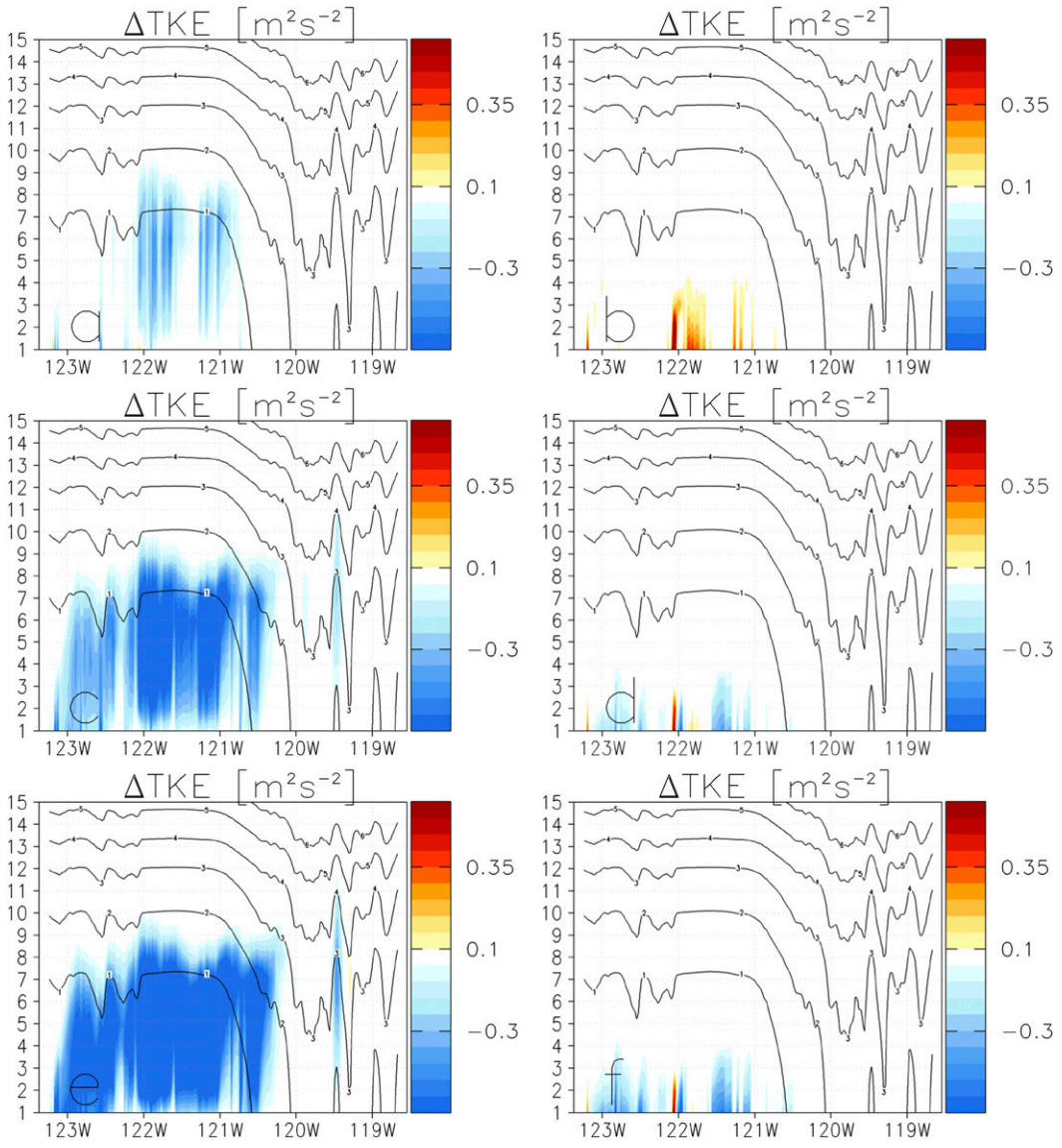

FIG. 14. As in Fig. 13, but the vertical cross section is calculated at 38.5°N.

nighttime hours—and therefore more directly tackles the effects of the UHI—are key themes of ongoing research. Including the influence of anthropogenic climate change impacts on large-scale circulation pattern changes likely to modify regional climate, with implications for air quality, also requires attention (Weaver et al. 2009). Future studies incorporating additional uncertainty due to urban canyon aspect ratio (Ching et al. 2009), differences in spatial distribution projections of population centers (Jones and O'Neill 2013), and various ways to account for features of surface and exchange processes within urban energy balance models (Grimmond et al. 2010; Song and Wang 2015) should lead to more precise estimates of urban-induced climate impacts.

Acknowledgments. M.G. greatly appreciates valuable discussions with C. P. Weaver on an earlier version of the manuscript and is also very grateful to P. E. Morefield and J. James for providing the ICLUS data. The comments from two anonymous reviewers have greatly improved the manuscript. M.G. was supported by NSF Grant EAR-1204774.

REFERENCES

Adachi, S. A., F. Kimura, H. Kusaka, T. Inoue, and H. Ueda, 2012: Comparison of the impact of global climate changes and urbanization on summertime future climate in the Tokyo metropolitan area. *J. Appl. Meteor. Climatol.*, **51,** 1441–1454, doi:10.1175/JAMC-D-11-0137.1.

Akbari, H., and H. D. Matthews, 2012: Global cooling updates: Reflective roofs and pavements. *Energy Build.,* **55,** 2–6, doi:10.1016/j.enbuild.2012.02.055.

——, S. Menon, and A. Rosenfeld, 2009: Global cooling: Increasing world-wide urban albedos to offset CO_2. *Climatic Change,* **94,** 275–286, doi:10.1007/s10584-008-9515-9.

Argüeso, D., J. P. Evans, L. Fita, and K. J. Bormann, 2014: Temperature response to future urbanization and climate change. *Climate Dyn.,* **42,** 2183–2199, doi:10.1007/s00382-013-1789-6.

Bierwagen, B. G., D. M. Theobald, C. R. Pyke, A. Choate, P. Groth, J. V. Thomas, and P. Morefield, 2010: National housing and impervious surface scenarios for integrated climate impact assessments. *Proc. Natl. Acad. Sci. USA,* **107,** 20 887–20 892, doi:10.1073/pnas.1002096107.

California Department of Finance, 2013: Report P-1 (County): State and county total population projections, 2010–2060. [Available online at http://www.dof.ca.gov/research/demographic/reports/projections/P-1/.]

Cayan, D. R., E. P. Maurer, M. D. Dettinger, M. Tyree, and K. Hayhoe, 2008: Climate change scenarios for the California region. *Climatic Change,* **87,** 21–42, doi:10.1007/s10584-007-9377-6.

Chester, M., S. Pincetl, Z. Elizabeth, W. Eisenstein, and J. Matute, 2013: Infrastructure and automobile shifts: Positioning transit to reduce life-cycle environmental impacts for urban sustainability goals. *Environ. Res. Lett.,* **8,** 015041, doi:10.1088/1748-9326/8/1/015041.

Ching, J., and Coauthors, 2009: National urban database and access portal tool. *Bull. Amer. Meteor. Soc.,* **90,** 1157–1168, doi:10.1175/2009BAMS2675.1.

Connors, J. P., C. S. Galletti, and W. T. Chow, 2013: Landscape configuration and urban heat island effects: Assessing the relationship between landscape characteristics and land surface temperature in Phoenix, Arizona. *Landscape Ecol.,* **28,** 271–283, doi:10.1007/s10980-012-9833-1.

Cordero, E. C., W. Kessomkiat, J. Abatzoglou, and S. A. Mauget, 2011: The identification of distinct patterns in California temperature trends. *Climatic Change,* **108,** 357–382, doi:10.1007/s10584-011-0023-y.

EPA, 2008a: Reducing urban heat islands: Compendium of strategies—Cool roofs. EPA, 28 pp. [Available online at http://www.epa.gov/heatisland/resources/pdf/CoolRoofsCompendium.pdf.]

——, 2008b: Reducing urban heat islands: Compendium of strategies—Green roofs. EPA, 26 pp. [Available online at http://www.epa.gov/heatisland/resources/pdf/GreenRoofsCompendium.pdf.]

Franco, G., D. R. Cayan, S. Moser, M. Hanemann, and M. A. Jones, 2011: Second California Assessment: Integrated climate change impacts assessment of natural and managed systems. *Climatic Change,* **109,** 1–19, doi:10.1007/s10584-011-0318-z.

Franklin, J., F. W. Davis, M. Ikegami, A. D. Syphard, L. E. Flint, A. L. Flint, and L. Hannah, 2013: Modeling plant species distributions under future climates: How fine scale do climate projections need to be? *Global Change Biol.,* **19,** 473–483, doi:10.1111/gcb.12051.

Georgescu, M., G. Miguez-Macho, L. T. Steyaert, and C. P. Weaver, 2009: Climatic effects of 30 years of landscape change over the Greater Phoenix, Arizona, region: 2. Dynamical and thermodynamical response. *J. Geophys. Res.,* **114,** D05111, doi:10.1029/2008JD010762.

——, M. Moustaoui, A. Mahalov, and J. Dudhia, 2011: An alternative explanation of the semiarid urban area ''oasis effect.'' *J. Geophys. Res.,* **116,** D24113, doi:10.1029/2011JD016720.

——, A. Mahalov, and M. Moustaoui, 2012: Seasonal hydroclimatic impacts of Sun Corridor expansion. *Environ. Res. Lett.,* **7,** 034026, doi:10.1088/1748-9326/7/3/034026.

——, M. Moustaoui, A. Mahalov, and J. Dudhia, 2013: Summer-time climate impacts of projected megapolitan expansion in Arizona. *Nat. Climate Change,* **3,** 37–41, doi:10.1038/nclimate1656.

——, P. E. Morefield, B. G. Bierwagen, and C. P. Weaver, 2014: Urban adaptation can roll back warming of emerging megapolitan regions. *Proc. Natl. Acad. Sci. USA,* **111,** 2909–2914, doi:10.1073/pnas.1322280111.

Grimmond, C. S. B., and T. R. Oke, 1999: Heat storage in urban areas: Local-scale observations and evaluation of a simple model. *J. Appl. Meteor.,* **38,** 922–940, doi:10.1175/1520-0450(1999)038<0922:HSIUAL>2.0.CO;2.

——, and Coauthors, 2010: The international urban energy balance models comparison project: First results from phase 1. *J. Appl. Meteor. Climatol.,* **49,** 1268–1292, doi:10.1175/2010JAMC2354.1.

Gurney, K. R., I. Razlivanov, Y. Song, Y. Zhou, B. Benes, and M. Abdul-Massih, 2012: Quantification of fossil fuel CO_2 emissions on the building/street scale for a large U.S. city. *Environ. Sci. Technol.,* **46,** 12 194–12 202, doi:10.1021/es3011282.

Hanna, S. R., and Coauthors, 2006: Detailed simulations of atmospheric flow and dispersion in downtown Manhattan: An application of five computational fluid dynamics models. *Bull. Amer. Meteor. Soc.,* **87,** 1713–1726, doi:10.1175/BAMS-87-12-1713.

Hayhoe, K., and Coauthors, 2004: Emissions pathways, climate change, and impacts on California. *Proc. Natl. Acad. Sci. USA,* **101,** 12 422–12 427, doi:10.1073/pnas.0404500101.

Jacobson, M. Z., 2001: GATOR-GCMM: 2. A study of daytime and nighttime ozone layers aloft, ozone in national parks, and weather during the SARMAP field campaign. *J. Geophys. Res.,* **106,** 5403–5420, doi:10.1029/2000JD900559.

Jones, B., and B. C. O'Neill, 2013: Historically grounded spatial population projections for the continental United States. *Environ. Res. Lett.,* **8,** 044021, doi:10.1088/1748-9326/8/4/044021.

Karl, T. R., H. F. Diaz, and G. Kukla, 1988: Urbanization: Its detection and effect in the United States climate record. *J. Climate,* **1,** 1099–1123, doi:10.1175/1520-0442(1988)001<1099:UIDAEI>2.0.CO;2.

Kaufmann, R. K., K. C. Seto, A. Schneider, Z. Liu, L. Zhou, and W. Wang, 2007: Climate response to rapid urban growth: Evidence of a human-induced precipitation deficit. *J. Climate,* **20,** 2299–2306, doi:10.1175/JCLI4109.1.

Keirstead, J., M. Jennings, and A. Sivakumar, 2012: A review of urban energy system models: Approaches, challenges and opportunities. *Renewable Sustainable Energy Rev.,* **16,** 3847–3866, doi:10.1016/j.rser.2012.02.047.

Kueppers, L. M., and M. A. Snyder, 2012: Influence of irrigated agriculture on diurnal surface energy and water fluxes, surface climate, and atmospheric circulation in California. *Climate Dyn.,* **38,** 1017–1029, doi:10.1007/s00382-011-1123-0.

Kusaka, H., and F. Kimura, 2004: Thermal effects of urban canyon structure on the nocturnal heat island: Numerical experiment using a mesoscale model coupled with an urban canopy model. *J. Appl. Meteor.,* **43,** 1899–1910, doi:10.1175/JAM2169.1.

LaDochy, S., R. Medina, and W. Patzert, 2007: Recent California climate variability: Spatial and temporal patterns in temperature trends. *Climate Res.,* **33,** 159–169, doi:10.3354/cr033159.

Lawrence, M. G., T. M. Butler, J. Steinkamp, B. R. Gurjar, and J. Lelieveld, 2007: Regional pollution potentials of megacities and other major population centers. *Atmos. Chem. Phys.,* **7,** 3969–3987, doi:10.5194/acp-7-3969-2007.

Lebassi, B., J. Gonzalez, D. Fabris, E. Maurer, N. Miller, C. Milesi, P. Switzer, and R. Bornstein, 2009: Observed 1970–2005 cooling of summer daytime temperatures in coastal California. *J. Climate,* **22,** 3558–3573, doi:10.1175/2008JCLI2111.1.

Li, J., M. Georgescu, P. Hyde, A. Mahalov, and M. Moustaoui, 2014: Achieving accurate simulations of urban impacts on ozone at high resolution. *Environ. Res. Lett.,* **9,** 114019, doi:10.1088/1748-9326/9/11/114019.

Lobell, D. B., and C. B. Field, 2011: California perennial crops in a changing climate. *Climatic Change,* **109,** 317–333, doi:10.1007/s10584-011-0303-6.

Mahmud, A., M. Tyree, D. Cayan, N. Motallebi, and M. J. Kleeman, 2008: Statistical downscaling of climate change impacts on ozone concentrations in California. *J. Geophys. Res.,* **113,** D21103, doi:10.1029/2007JD009534.

Mills, G., 2007: Cities as agents of global change. *Int. J. Climatol.,* **27,** 1849–1857, doi:10.1002/joc.1604.

Moser, S., G. Franco, S. Pittiglio, W. Chou, and D. Cayan, 2009: The future is now: An update on climate change science impacts and response options for California. California Climate Change Center Rep. CEC-500-2008-071, 114 pp. [Available online at http://www.energy.ca.gov/2008publications/CEC-500-2008-071/CEC-500-2008-071.PDF.]

Myint, S. W., E. A. Wentz, A. J. Brazel, and D. A. Quattrochi, 2013: The impact of distinct anthropogenic and vegetation features on urban warming. *Landscape Ecol.,* **28,** 959–978, doi:10.1007/s10980-013-9868-y.

Oleson, K. W., G. B. Bonan, and J. Feddema, 2010: Effects of white roofs on urban temperature in a global climate model. *Geophys. Res. Lett.,* **37,** L03701, doi:10.1029/2009GL042194.

Pierce, D. W., and Coauthors, 2013: Probabilistic estimates of future changes in California temperature and precipitation using statistical and dynamical downscaling. *Climate Dyn.,* **40,** 839–856, doi:10.1007/s00382-012-1337-9.

Sailor, D. J., 2008: A green roof model for building energy simulation programs. *Energy Build.,* **40,** 1466–1478, doi:10.1016/j.enbuild.2008.02.001.

Salamanca, F., M. Georgescu, A. Mahalov, M. Moustaoui, and M. Wang, 2014: Anthropogenic heating of the urban environment due to air conditioning. *J. Geophys. Res. Atmos.,* **119,** 5949–5965, doi:10.1002/2013JD021225.

Santamouris, M., A. Synnefa, and T. Karlessi, 2011: Using advanced cool materials in the urban built environment to mitigate heat islands and improve thermal comfort conditions. *Sol. Energy,* **85,** 3085–3102, doi:10.1016/j.solener.2010.12.023.

Shepherd, J. M., 2005: A review of current investigations of urban-induced rainfall and recommendations for the future. *Earth Interact.,* **9,** doi:10.1175/EI156.1.

Skamarock, W. C., and J. B. Klemp, 2008: A time-split nonhydrostatic atmospheric model for weather research and forecasting applications. *J. Comput. Phys.,* **227,** 3465–3485, doi:10.1016/j.jcp.2007.01.037.

Song, J., and Z.-H. Wang, 2015: Interfacing the urban land–atmosphere system through coupled urban canopy and atmospheric models. *Bound.-Layer Meteor.,* doi:10.1007/s10546-014-9980-9, in press.

Stewart, I. D., and T. R. Oke, 2012: Local climate zones for urban temperature studies. *Bull. Amer. Meteor. Soc.,* **93,** 1879–1900, doi:10.1175/BAMS-D-11-00019.1.

Synnefa, A., and M. Santamouris, 2012: Advances on technical, policy and market aspects of cool roof technology in Europe: The Cool Roofs project. *Energy Build.,* **55,** 35–41, doi:10.1016/j.enbuild.2011.11.051.

Taha, H., 2008a: Meso-urban meteorological and photochemical modeling of heat island mitigation. *Atmos. Environ.,* **42,** 8795–8809, doi:10.1016/j.atmosenv.2008.06.036.

——, 2008b: Urban surface modification as a potential ozone air-quality improvement strategy in California: A mesoscale modelling study. *Bound.-Layer Meteor.,* **127,** 219–239, doi:10.1007/s10546-007-9259-5.

USDA, 2012: California agricultural statistics review: 2012–2013. USDA National Agricultural Statistics Service, Pacific Region–California, 131 pp. [Available online at www.cdfa.ca.gov/statistics/pdfs/2013/FinalDraft2012-2013.pdf.]

von Storch, H., and F. W. Zwiers, 2002: *Statistical Analysis in Climate Research.* Cambridge University Press, 484 pp.

Weaver, C. P., and Coauthors, 2009: A preliminary synthesis of modeled climate change impacts on U.S. regional ozone concentrations. *Bull. Amer. Meteor. Soc.,* **90,** 1843–1863, doi:10.1175/2009BAMS2568.1.

Wu, J. J., 2008: Making the case for landscape ecology: An effective approach to urban sustainability. *Landscape J.,* **27,** 41–50, doi:10.3368/lj.27.1.41.

Yang, J., and Z.-H. Wang, 2014: Physical parameterization and sensitivity of urban hydrological models: Application to green roof systems. *Build. Environ.,* **75,** 250–263, doi:10.1016/j.buildenv.2014.02.006.

Zhao, C., A. E. Andrews, L. Bianco, J. Eluszkiewicz, A. Hirsch, C. MacDonald, T. Nehrkorn, and M. L. Fischer, 2009: Atmospheric inverse estimates of methane emissions from central California. *J. Geophys. Res.,* **114,** D16302, doi:10.1029/2008JD011671.

Zhao, Z., S. H. Chen, M. J. Kleeman, and A. Mahmud, 2011: The impact of climate change on air quality–related meteorological conditions in California. Part II: Present versus future time simulation analysis. *J. Climate,* **24,** 3362–3376, doi:10.1175/2010JCLI3850.1.